



HAL
open science

Oxidation Extent of the Upper Mantle by Subducted Slab and Possible Oxygen Budget in Deep Earth Inferred From Redox Kinetics of Olivine

Chengcheng Zhao, Takashi Yoshino, Baohua Zhang

► **To cite this version:**

Chengcheng Zhao, Takashi Yoshino, Baohua Zhang. Oxidation Extent of the Upper Mantle by Subducted Slab and Possible Oxygen Budget in Deep Earth Inferred From Redox Kinetics of Olivine. *Journal of Geophysical Research: Solid Earth*, 2022, 127, 10.1029/2021JB022977 . insu-03708911

HAL Id: insu-03708911

<https://insu.hal.science/insu-03708911>

Submitted on 22 Mar 2023

HAL is a multi-disciplinary open access archive for the deposit and dissemination of scientific research documents, whether they are published or not. The documents may come from teaching and research institutions in France or abroad, or from public or private research centers.

L'archive ouverte pluridisciplinaire **HAL**, est destinée au dépôt et à la diffusion de documents scientifiques de niveau recherche, publiés ou non, émanant des établissements d'enseignement et de recherche français ou étrangers, des laboratoires publics ou privés.

Copyright

JGR Solid Earth

RESEARCH ARTICLE

10.1029/2021JB022977

Key Points:

- Redox kinetics of olivine were investigated by diffusion couple method at 1 GPa and 1,373–1,573 K
- Below $\Delta\text{FMQ} + 1$, redox process is controlled by O grain boundary diffusion, while above that, by H diffusion related with Mg vacancy
- Slow redox rate limits homogenization of subducted slab with mantle. A highly underestimated oxygen reservoir may be present in deep Earth

Supporting Information:

Supporting Information may be found in the online version of this article.

Correspondence to:

C. Zhao,
cczhao_zhao@outlook.com

Citation:

Zhao, C., Yoshino, T., & Zhang, B. (2022). Oxidation extent of the upper mantle by subducted slab and possible oxygen budget in deep Earth inferred from redox kinetics of olivine. *Journal of Geophysical Research: Solid Earth*, 127, e2021JB022977. <https://doi.org/10.1029/2021JB022977>

Received 6 AUG 2021

Accepted 31 JAN 2022

Oxidation Extent of the Upper Mantle by Subducted Slab and Possible Oxygen Budget in Deep Earth Inferred From Redox Kinetics of Olivine

Chengcheng Zhao^{1,2} , Takashi Yoshino¹ , and Baohua Zhang³ 

¹Institute for Planetary Materials, Okayama University, Misasa, Japan, ²Laboratoire Magmas et Volcans CNRS, IRD, OPGC, Université Clermont Auvergne, Clermont-Ferrand, France, ³Key Laboratory of Geoscience Big Data and Deep Resource of Zhejiang Province, Institute of Geology and Geophysics, School of Earth Sciences, Zhejiang University, Hangzhou, China

Abstract Redox input by subducted slab into mantle is important for deep cycle and isotopic evolution of volatile elements, whose stable forms are controlled by redox state. Given reduced condition in lower part of the upper mantle, taking redox budget from lithospheric mantle into consideration is crucial in redefining redox state there. To constrain to which extent subducted slab modified redox state of the uppermost mantle and how much oxygen budget slab carried into deep Earth, we investigated redox kinetics of olivine adopting diffusion couple method at 1 GPa and 1,373–1573 K in a piston cylinder apparatus. It is found that redox process in olivine is diffusion-controlled, and diffusing on the order of 10^{-12} m²/s at 1473 K. Oxidation process in reduced part is oxygen fugacity ($f\text{O}_2$)-independent with activation enthalpy of 235 ± 56 kJ/mol, while reduction process in oxidized part is $f\text{O}_2$ -dependent with an $f\text{O}_2$ exponent of 2/5. Diffusion profile analysis reveals that for magnetite-free couple, redox process is controlled by oxygen grain boundary diffusion (GBD) below $\Delta\text{FMQ} + 1$, and rate-limited by faster species which might be hydrogen related Mg vacancy above $\Delta\text{FMQ} + 1$. However, for magnetite-bearing couple, oxygen GBD dominates redox process across wide $f\text{O}_2$ range. The extremely slow rate limits the homogenization of the slab with surrounding mantle so that redox state of the uppermost mantle remains unchanged in the past 3.5 Gyrs. A highly underestimated oxygen reservoir may have formed in deep Earth, when subducted slab transports oxidized components to region deeper than the mantle transition zone.

Plain Language Summary As oxidized slabs continue subducting into mantle, redox exchange proceeds between slabs and the surrounding mantle. Knowledge of redox kinetics of olivine is essential for understanding redox evolution of the uppermost mantle in the Earth's history and unraveling redox budget in slab residues that brought into deeper Earth. In this study, we conducted a series of diffusion experiments to determine rates of redox processes in olivine aggregates under high pressure and high temperature. Our results show that diffusion-controlled redox processes in olivine aggregates are extremely slow. The extent of surrounding upper mantle which can be oxidized by slabs is very limited. The unchanging redox state of the uppermost mantle is not caused by its infinite redox capacity as previously supposed but due to its inability to digest oxidized components efficiently. Being not fully absorbed by the uppermost mantle, the oxidized slabs tend to transport a considerable amount of oxidized components into deeper mantle with further subducting.

1. Introduction

How redox state of the uppermost mantle has evolved through geological time has long been a focus of hot debate. It is expected to be altered because of continuous input of oxidized components by subduction process. However, concentrations of Cr, V, and the V/Sc ratio of the oldest known rocks showed that oxygen fugacity ($f\text{O}_2$) of the uppermost mantle had remained at approximately fayalite-magnetite-quartz (FMQ) over past 3.5 Gyrs (Canil, 2002; Li & Lee, 2004). It is possible that oxidized materials might be prevented to be incorporated into deeper mantle, if they were to oxidize mantle wedge during subduction (Brounce et al., 2015; Parkinson & Arculus, 1999). However, Zn/Fe_T signature in primitive arc magmas originated from mantle wedge indicated that they were not generated in oxidized environments, suggesting that redox state of mantle wedge was not significantly altered by subducted oxidized materials (Lee et al., 2010). Thus, the question is how the subducted oxidized materials behave. Oxidized arc rocks or gases originated from mantle wedge could bring dissolved oxidized components back to the Earth's surface (Brounce et al., 2014; Kelley & Cottrell, 2009). Nevertheless,

$\text{Fe}^{3+}/\Sigma\text{Fe}$ ratios of subducted materials from the Mariana subduction zone demonstrated that significant amount of O_2 added to the subducted crust by several processes is not output by arc volcanism (Brounce et al., 2019). Therefore, oxide components are likely to remain in subducted slabs and been transported into deeper mantle beyond subduction zones (Kadik, 1997; Kasting et al., 1993).

The extent of mantle oxidized by subducted slab can be assessed by calculating input and output of main redox-sensitive elements such as Fe, C and S (Evans, 2012; Evans & Powell, 2015; Evans & Tomkins, 2011; Lécuyer & Ricard, 1999). Fe^{3+} flux from sediments, altered oceanic crust and partially serpentinized lithospheric mantle is $15 \pm 13 \times 10^{12}$ mol/y, which is $\sim 27\%$ of the total Fe flux (Evans, 2012). Redox budget of a rock is defined as the number of moles of electrons which needs to be added to the rock to reach a reference state (Evans, 2006), which is usually considered to be Fe^{2+} for Fe in the uppermost mantle. Thus, redox budget of Fe in subducting slab was calculated to be $15 \pm 13 \times 10^{12}$ mol/y. Because more electrons are needed to bring C and S in slabs to their reference states, their redox budget to deeper mantle was increasingly investigated and emphasized (Galvez et al., 2013; Kerrick & Connolly, 2001; Schwarzenbach et al., 2018; Sverjensky et al., 2014).

However, ability of Fe in the slab as redox budget is underestimated when we consider the fact that $f\text{O}_2$ relative to FMQ decreases towards deep Earth (Frost & McCammon, 2008). In the uppermost mantle, $f\text{O}_2$ is near FMQ equilibrium, which is determined by Fe^{2+} - Fe^{3+} equilibrium in silicate minerals. However, from lower half of the upper mantle (~ 240 km) to the lower mantle, $f\text{O}_2$ decreases from near iron-wüstite (IW) equilibrium to ~ 1.5 log units below that, producing metals with compositions from Ni-rich to almost pure iron (Rohrbach & Schmidt, 2011). P-wave tomography revealed that most of slabs stagnated above the 660 km discontinuity or trapped in the uppermost lower mantle (600–1,000 km; Fukao & Obayashi, 2013), demonstrating the slabs reached far beyond the uppermost mantle to the reduced deeper mantle. Therefore, it is possible that Fe in subducted slab there could be present in the form of metallic phase, at least partially, at depth shallower than the 410 km seismic discontinuity, if a dynamic equilibrium achieves with surrounding mantle. And metallic iron should be referred as the reference state of Fe for slabs at depth below 240 km (Rohrbach & Schmidt, 2011). In this case, both Fe^{2+} and Fe^{3+} contribute to redox budget of subducted slabs. Previous estimation of net total input of Fe was $55 \pm 13 \times 10^{12}$ mol/y, occupying up to 90% of multi-valence element fluxes (Evans, 2006), whose result excluded Fe^{2+} contribution from un-serpentinized lithospheric mantle. In the present study, Fe flux (mainly in the form of Fe^{2+}) from un-serpentinized lithospheric mantle, whose volume is usually 5–20 times thicker than serpentinized one (Gorman et al., 2006; Rupke et al., 2004), would be added to better constrain redox budget of slabs, which is previously greatly underestimated.

Olivine and pyroxene are main constituent minerals in lithospheric mantle of slabs. During subduction, when iron in olivine is reduced to metallic phase, O_2 will be released and $f\text{O}_2$ of surrounding mantle will be elevated. Experimental investigation on redox kinetics of olivine is necessary, in order to accurately evaluate oxidation extent of the surrounding mantle and redox budget of Fe brought by slab. The hypothesis whether the upper mantle represents an infinite redox reservoir and consumes all redox input supplied by slab so that a nearly constant $f\text{O}_2$ of the upper mantle is maintained over geological time (Lee et al., 2010; Rohrbach & Schmidt, 2011) can be tested. In this study we employed diffusion couple method to investigate redox kinetics of Pt-doped olivine aggregates (Pt as oxygen sensor) at 1,373–1,573 K and 1 GPa under water undersaturated condition using piston cylinder apparatus. Diffusion coefficient was calculated from $f\text{O}_2$ profile. Mechanisms dominating reduction and oxidation processes are discussed. Assuming water undersaturated condition, we calculate the maximum diffusion lengths through redox process and present the maximum oxidation extent of the upper mantle that can be altered by subducting slabs. Finally, a total redox budget of Fe brought by slabs into deeper Earth every year is estimated, taking metallic iron as the reference state.

2. Methods

2.1. Sample Preparation

Reagent grade MgO , SiO_2 and Fe_2O_3 with stoichiometric olivine composition were mixed in an agate mortar. 3 wt% SiO_2 powder was added as silica buffer. The powder mixture was pressed into thin disks and baked at 1,573 K in a gas mixture furnace for 4 hr with CO_2 and H_2 gas flow controlled at $f\text{O}_2$ near Ni-NiO (NNO) equilibrium which is approximate to FMQ buffered condition or at $f\text{O}_2$ near IW buffered condition. After baking, olivine was identified as the main phase with small amount of orthopyroxene (Opx) using X-ray diffraction (XRD)

analysis. Oxygen sensor of 5 wt% Pt powder was added and fully mixed with pre-synthesized silica-buffered olivine powder, which was baked at the same condition in the gas mixture furnace for another 4 hr. After quench, Pt-doped olivine powders at oxidized (near NNO buffer) and reduced (near IW buffer) conditions were obtained.

Sintering of Pt-doped olivine aggregate was performed at 1,373–1,573 K and 1 GPa in an end-loaded piston-cylinder apparatus using conventional 3/4 Talc/Pyrex assembly. Mineral assemblage equilibria for precise pressure and temperature calibration were not performed. Pressure was generated according to the theoretical pressure-load relationship that P (kb) = $0.1090 \times \text{load}$, assuming 3% friction correction. S type thermocouple was used to monitor temperature whose uncertainty was within ± 2.5 K (<https://www.thermocoupleinfo.com>). No correction for pressure effects on EMF was applied. Temperature difference of the sample part was controlled within 15 K by using a tapered heater. To obtain dry aggregate, starting powder was kept at 473 K in a vacuum furnace before it was loaded into Ni or Mo capsule which was used for keeping the NNO or IW buffered condition of starting powders respectively, while absorbing possible moisture during keeping. To prevent generation of cracks during decompression, Pyrex glass tube was used outside Ni/Mo capsule and sample was decompressed to room pressure at 1,073 K after sintering at the target temperature (Table S1 in Supporting Information S1).

After recovery, the sintered sample was cut into several pieces. Micro-texture was observed by scanning electron microscope (SEM) using one piece from them. Volume fraction of Opx in olivine matrix was estimated to be 10–14 vol% using ImageJ on SEM images. Average grain size of olivine matrix was counted to be 2–4 μm (Table S1 in Supporting Information S1), using intercept method (Mendelson, 1969) with the relation $d = cL$ where d is grain size, L is length of intercept, and c is a constant of 1.56. Re-equilibrating of Pt particles with olivine during sintering at elevated pressure and lowered temperature (compared with synthesis conditions at gas mixture furnace) causes either breakdown of olivine into Fe and Opx and release of oxygen, or the opposite reaction direction, as indicated below:



Thus, local $f\text{O}_2$ of sample can be evaluated from changing Fe content in Pt alloys (Faul et al., 2017), which monitors real-time $f\text{O}_2$. To evaluate whether a new steady-state of $f\text{O}_2$ was reached across the sample, chemical composition of more than 20 points of Pt alloys and neighboring olivine grains was measured by electron microprobe (EPMA) from near Ni/Mo capsule to the center part on cross section of sliced piece. Their oxygen fugacities were calculated following method described in Faul et al. (2017). The almost constant oxygen fugacity (Figure S1 in Supporting Information S1) indicates that sintered sample has reached a new equilibrium state corresponding to varied pressure and temperature in the piston cylinder apparatus (Table S1 in Supporting Information S1). For oxidized samples, except one sample containing significant amount of magnetite which shows near 10 log units higher $f\text{O}_2$ than IW buffer, others are magnetite-free and show $f\text{O}_2$ 4.4–7.6 log units higher than that. For the reduced samples, $f\text{O}_2$ was determined to be 1.1–1.6 log units higher than IW buffer (Table S1 in Supporting Information S1).

2.2. Diffusion Experiment and Sample Characterization

Diffusion couple method was used to investigate redox kinetics of olivine. After removing metal capsule, both oxidized and reduced Pt-doped polycrystalline olivine disks with about 4 mm-diameter and 1 mm-thickness were surface-polished and stacked face to face, referred as a diffusion couple. The couple was fully covered with 10 μm thick Pt foil to avoid reaction with surrounding MgO. Diffusion profile was confirmed to be absent in zero-time run (Figure S5 in Supporting Information S1) where experiment was quenched by shutting down power supply once temperature was increased to 1473 K. Time-series diffusion runs with different duration from 5 to 18 hr were performed at 1,473 K and 1 GPa (Table 1), the same temperature and pressure with their sintering conditions (Table S1 in Supporting Information S1). To obtain activation enthalpy, two additional experiments at 1,373 and 1,573 K were also performed (Table 1).

After annealing, recovered couple was cut into two halves at center, normal to the initial contact interface. One half of the sample was used for SEM and EPMA measurement. In most cases, initial interface in diffusion couples could be easily identified because of mechanical separation of two parts after decompression, while some were invisible (Figure 1). A homogeneous texture with average grain size of 2–5 μm was observed (Table 1). In most

Table 1
Experimental Summary of Diffusion Experiment Using Piston-Cylinder Apparatus

Run no.	Starting sample	T (K)	Duration (h)	Capsule	Grain size (μm)	Grain growth (%)	log D (m^2/s)
PC702	PC699 + PC686	1,473	0	Pt foil	/	/	/
PC703	PC699 + PC686	1,473	5	Pt foil	O: 4.5 (2.5) R: 2.3 (1.2)	37 2	-12.20 (8)
PC698	PC665 + PC674	1,473	13	Pt foil	O: 3.9 (2.3) R: 3.1 (1.7)	26 16	-12.44 (3)
PC715	PC714	1,473	18	Pt foil	O: 4.8 (3.0) R: 2.7 (1.4)	93 15	-12.64 (2)
PC689 ^a	PC687 ^a + PC686	1,473	12	Pt foil	/	/	-12.40 (4)
PC711	PC710	1,373	30	Pt foil	O: 2.5 (1.4) R: 2.2 (1.2)	9 -5	-12.97 (4)
PC719	PC718	1,573	3	Pt foil	O: 4.2 (2.3) R: 4.2 (2.8)	111 14	-11.83 (4)

Note. “O” and “R” in the column of grain size mean oxidized half and reduced half of diffusion couple respectively. “-5” in column of Growth (%) means the grain size after diffusion experiment is the same with that before diffusion experiment, that is, no grain growth occurs. Number in parenthesis is the calculated standard deviation of corresponding data. “/” in PC702 and PC689 means corresponding properties is not calculated.

^amagnetite-bearing sample or diffusion couple.

cases no significant grain growth occurred (Table 1 and Table S1 in Supporting Information S1), neither obvious change of volume fraction of orthopyroxene. Fe content in Pt alloy and chemical composition of neighboring olivine across diffusion couple were acquired using EPMA from the center part of the diffusion couple (red region in Figure 1) to minimize possible influence from outer Pt foil. $f\text{O}_2$ profile was plotted as a function of distance from the contact interface of oxidized and reduced parts (Figure 2).

The other half was double-polished to 100–300 μm thickness for infrared (IR) spectroscopy measurement to determine water content. A JASCO IRT5200IMPY Fourier-transform IR (FTIR) spectrometer with an aligned transmission geometry was used under vacuum condition. IR spectra were acquired with an aperture size of 100×100 and an accumulation of 128 scans. At least 3–5 different points were measured for each sample. After baseline correction and thickness normalization, the Paterson calibration (Paterson, 1982) was adopted to obtain water content with an integration range of $3,000\text{--}3,730 \text{ cm}^{-1}$ and an orientation factor of 1/2.

2.3. Determination of Diffusion Coefficient

Along diffusion profile, $f\text{O}_2$ gradient led to chemical reaction between Pt oxygen sensor and surrounding olivine grains until a new local $f\text{O}_2$ equilibrium was reached. Iron contents in olivine grains are shown to be nearly constant (Figure S2 in Supporting Information S1), whereas the iron content in Pt alloy (X_{Fe}) is more sensitive and has a strong inverse correlation with $f\text{O}_2$ (Fig. S3 in Supporting Information S1). So X_{Fe} was taken as the indicator of local $f\text{O}_2$ variation during redox process. To determine diffusion coefficient, redox process in olivine aggregate was assumed to be one-dimension diffusion in semi-infinite space. A theoretically perfect diffusion profile was difficult to obtain during experiment. However, by carefully confining the fitting range which reflected redox kinetics of interest, artifacts from other processes could be removed and their influences on diffusivity were estimated to be not significant. Tail in the reduced part caused by Fe loss to Pt foil gives rise to an artifact that the original $f\text{O}_2$ was not maintained during diffusion. However, from the aspect of redox kinetics revealed by diffusion couple method, the judging criterium is whether the minimum $f\text{O}_2$ after diffusion overlaps with the initial one. Close inspection shows that the boundary condition of semi-infinite media for the reduced part is satisfied within error (Figure 2). For the oxidized part, most runs maintain their initial $f\text{O}_2$ during diffusion except some. For PC719, the elevated $f\text{O}_2$ was resulted from oxidizing environment confined by Pt capsule, which was removed in later calculation (Figure 3f). For PC689, it is reasonable to set the final $f\text{O}_2$ as one end of diffusion profile since

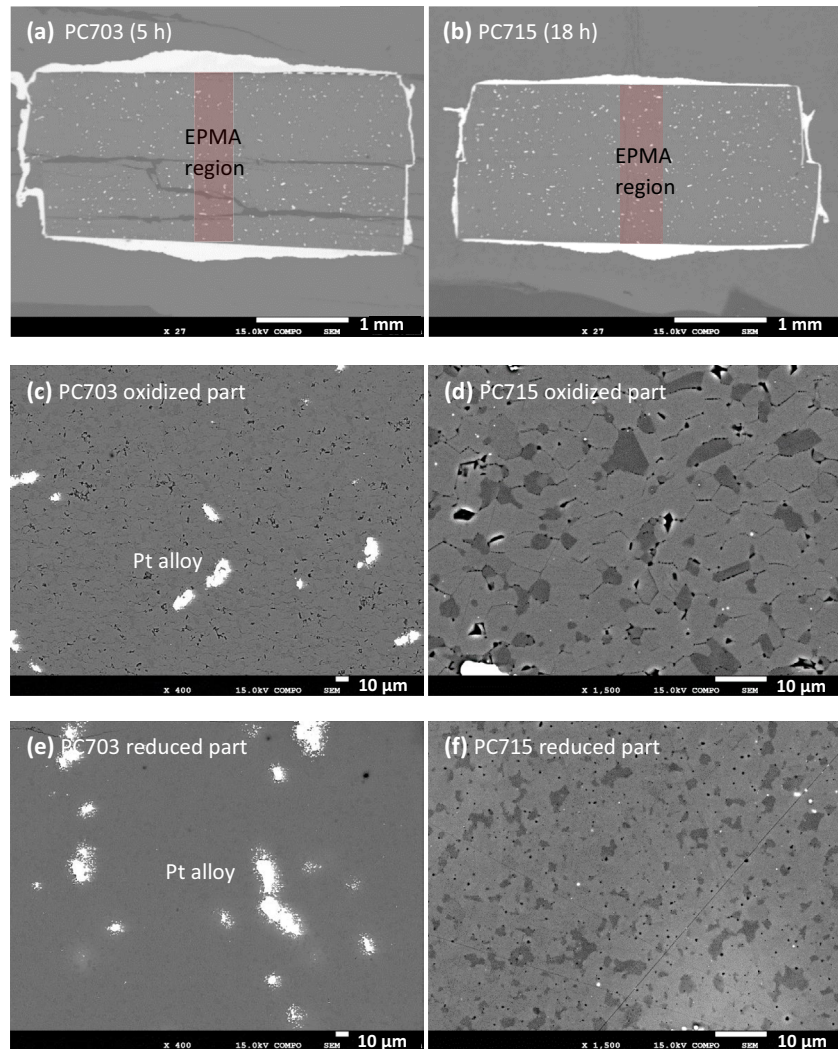


Figure 1. Typical texture of diffusion couple after diffusion annealing with different durations at 1,473 K. Bright grains in (c) (e) are Pt alloy, and dark gray grains in (d) (f) are opx. Volume fraction of orthopyroxene does not change much after annealing. Grain boundaries in oxidized part becomes visible after annealing while those in reduced part still not obvious. Length scale is annotated in the bottom right corner in every subfigure.

decomposition of magnetite, which provided an infinite oxygen reservoir, was ahead of reduction of olivine (see Results part below for detailed information). For PC715, it seems that fO_2 flattened out beyond the sample with only several points lying in the initial fO_2 region. However, the obtained diffusivity is in good agreement with other runs at 1473 K (Figure 4), indicating negligible influence.

Diffusion profile of X_{Fe} in Pt alloy versus distance from the interface for magnetite-free couple (Figure 3) shows asymmetric feature as a consequence of concentration-dependent diffusion. After removing data points caused by other processes aforementioned, Boltzmann-Matano method was used to obtain diffusion coefficient (Matano, 1933). First, considering the asymmetric feature of diffusion profile, raw data was fitted to the equation below:

$$C(x) = A_1 + (A_2 - A_1) \left[\frac{p}{1 + 10^{(\text{Log}x_1 - x)h_1}} + \frac{1 - p}{1 + 10^{(\text{Log}x_2 - x)h_2}} \right] \quad (3)$$

where x is the distance of data point from the initial interface, $C(x)$ is the mole fraction of Fe in Pt alloy expressed as X_{Fe} , others are fitting parameters. Then position of Matano interface x was determined where it satisfied equation below:

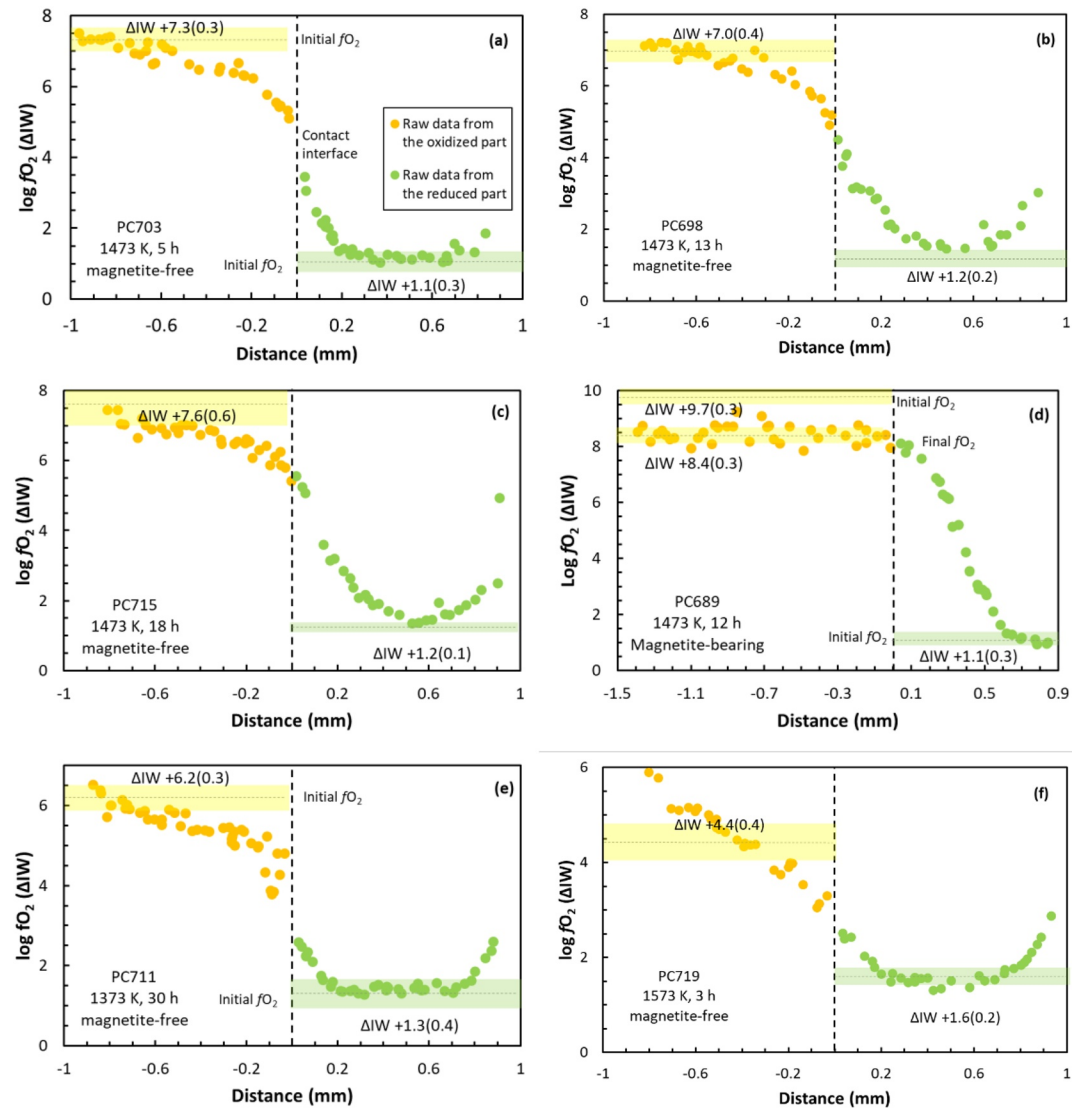


Figure 2. Oxygen fugacity profiles as a function of distance from the initial contact interface at 1,373–1,573 K. Yellow and green circles are f_{O_2} for oxidized and reduced parts in diffusion couple respectively. Horizontal dotted lines are the initial f_{O_2} before diffusion. Yellow and green shaded areas are calculated standard deviation.

$$\int_{C_1}^{C_2} x dC = 0 \quad (4)$$

where C_1 and C_2 are the minimum and maximum X_{Fe} in the diffusion profile, respectively. Finally, diffusion coefficient was calculated using equation below to obtain iron content-dependent diffusivity:

$$D = -\frac{1}{2t} \left(\frac{dx}{dC} \right) \int_{C_1}^C x dC, \quad (5)$$

where C is the normalized iron content at position x , D is the diffusion coefficient.

Although magnetite-bearing couple appeared to be composition-independent at first sight, Boltzmann-Matano method was still adopted to allow for possible subtle asymmetric diffusion. As shown in Figure 2d, the oxidized part of the magnetite-bearing couple shows that f_{O_2} was dropped by ~ 1.3 log unit without clear diffusion profile.

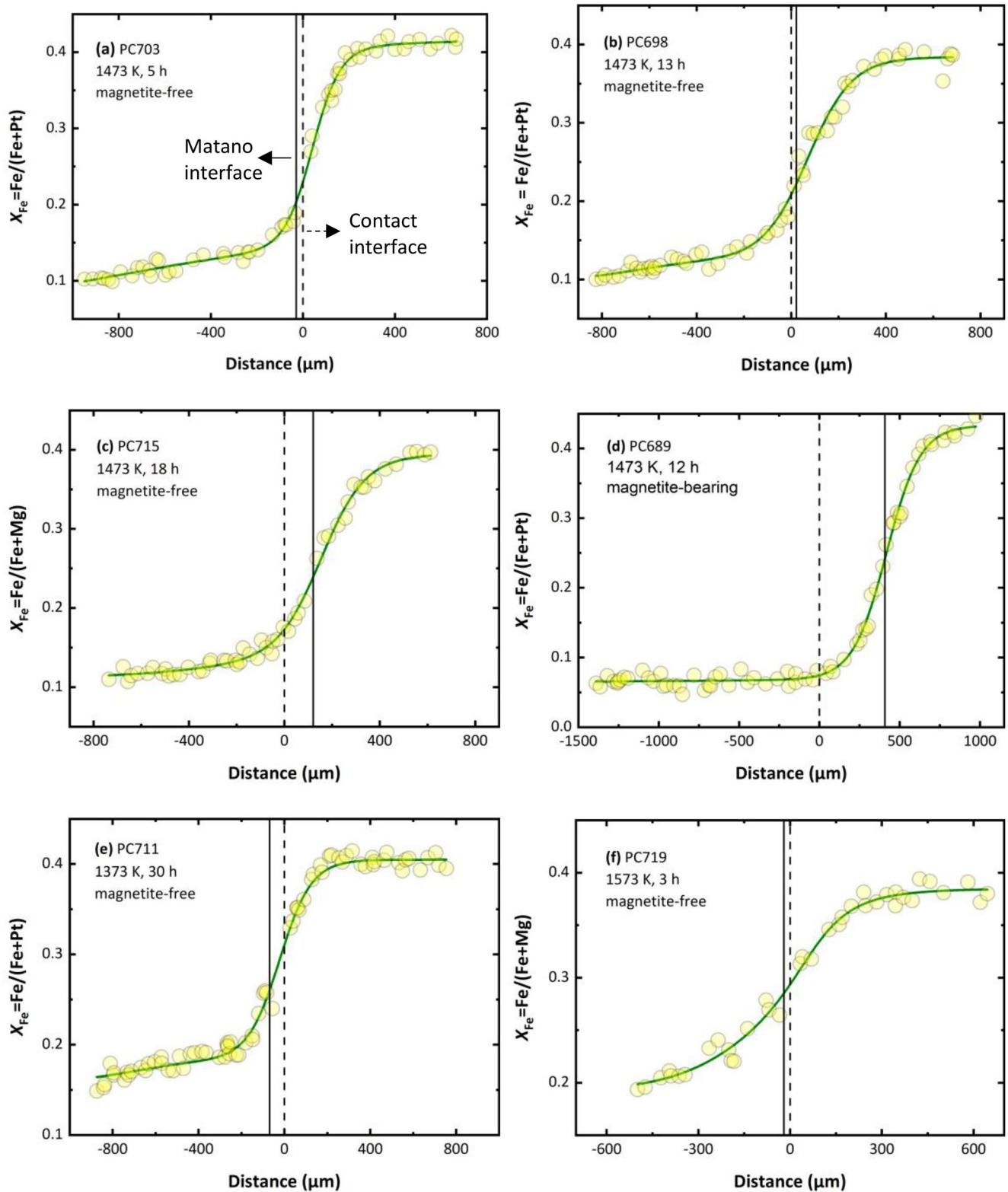


Figure 3. Diffusion profile of iron content in Pt alloy (X_{Fe}) versus distance from the initial contact interface from 1,373 to 1,573 K with different durations. Yellow filled circles are iron mole fractions entrained in Pt alloy. Green line is the fitting line. Vertical dashed line indicates the initial contact interface and solid line the Matano interface.

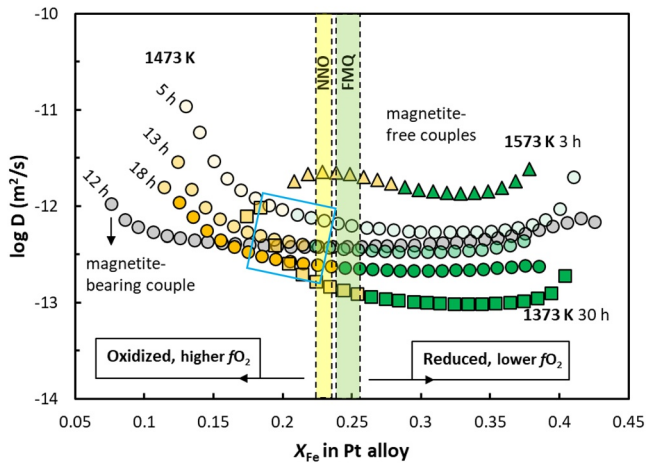


Figure 4. Diffusion coefficient as a function of iron content in Pt alloy (X_{Fe}). Yellow and green symbols (triangles and circles) indicate diffusivities in the initially oxidized and reduced parts in magnetite-free couples respectively. Gray circles represent diffusivities from magnetite-bearing couple. Points in blue solid rectangle are used to calculate fO_2 -exponent p . Vertical yellow and light green shaded regions indicate fO_2 at NNO and FMQ equilibrium at 1,373–1,573 K and 1 GPa, respectively.

fO_2 profile as function of distance from initial contact interface from 1,373 to 1,573 K (Figure 2) indicate one-dimension asymmetric diffusion in infinite space for magnetite-free couple. In X_{Fe} profile, only data points caused by redox kinetics in olivine is plotted (Figure 3). In the left side, X_{Fe} increases mildly over long distance (total length of sample thickness), then increases rapidly until the profile reaches its end and levels out in the right side. Usually longer diffusion length was observed in the oxidized part. Shift of Matano interface for magnetite-free couple is negligible, especially for runs with short duration (Figures 3a and 3b), indicating similar redox kinetics in two parts. With increasing duration, larger shift is observed (Figure 3c).

Diffusion coefficients obtained against X_{Fe} show that diffusivity increases with increasing temperature (Figure 4), while time-series runs annealed at 1473 K shows almost constant diffusivities within 4% deviation (Supplementary Figure S6 in Supporting Information S1). In magnetite-free couple, two different features can be identified. One is fO_2 -independent diffusivity below NNO buffer in the reduced part shown as nearly constant line after removing obviously up-bending diffusivities at reduced end (Figure 4). The other is fO_2 -dependent diffusivity in the oxidized part above NNO buffer shown as increased diffusivity with decreasing X_{Fe} (increasing fO_2). For the former, averaged diffusion coefficient below NNO buffer, excluding up-bend points influenced by Pt capsule, is used as the final value (Table 1). Activation enthalpy (ΔH) is obtained (Figure 5) through fitting of diffusion coefficient (D) to the Arrhenius equation:

$$D = D_0 \exp\left(-\frac{\Delta H}{kT}\right), \quad (6)$$

where D_0 is pre-exponential factor, k is the Boltzmann constant, T is absolute temperature. It yields $\Delta H = 235 \pm 56$ kJ/mol and $\log D_0 = -4.07 \pm 1.98$ m²/s. For the latter, a linear relationship is found at 1473 K (blue line rectangle in Figure 4) with the fO_2 -exponent p calculated to be 2/5 following the equation $D = D_0 f_{O_2}^p \exp\left(-\frac{\Delta H}{kT}\right)$.

In magnetite-bearing couple, diffusivity is fO_2 -independent across the entire fO_2 range (Figure 4), thus an averaged value over the whole fO_2 range

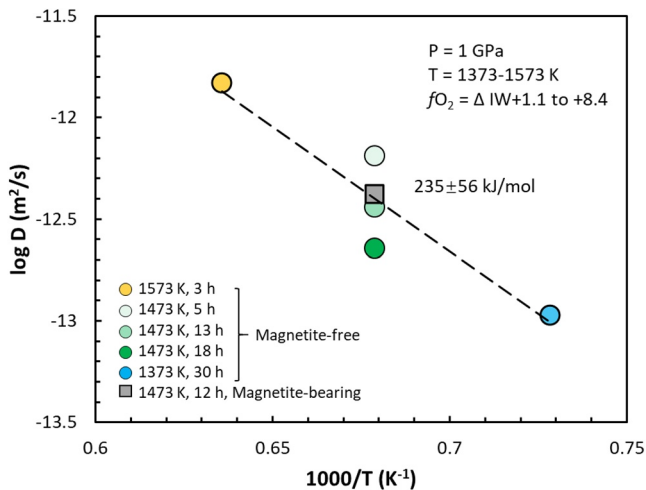


Figure 5. Diffusion coefficient as a function of reciprocal temperature. Yellow, green and blue colored circles are from averaged diffusivities in the reduced part of magnetite-free couples, with fitting line shown in dashed black line. Gray square is averaged diffusivity from magnetite-bearing couple.

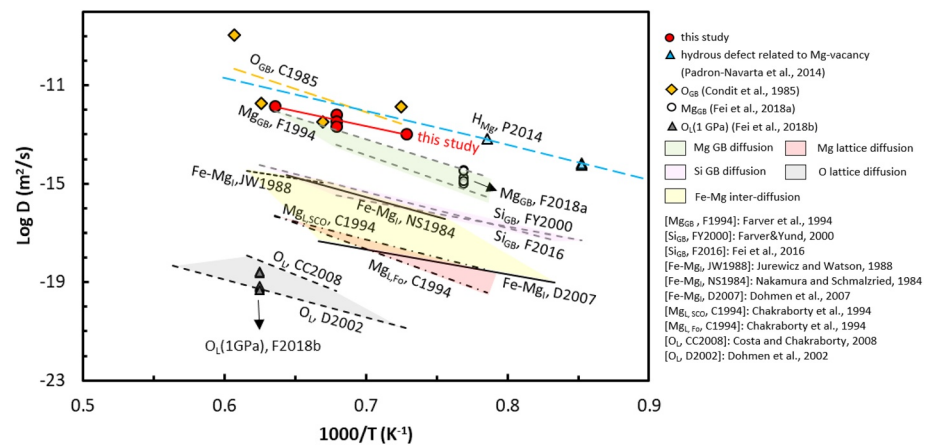


Figure 6. Diffusion coefficient in oxidation process below NNO buffer compared with diffusivities of other elements in olivine. Green region indicates Mg grain boundary diffusion, yellowish region Fe-Mg interdiffusion, pink region Mg lattice diffusion and gray region oxygen lattice diffusion. Except one data marked 1 GPa, others are obtained at room pressure.

(excluding up-bend end points) was used in later calculation. No diffusion is observed in the oxidized part, but within the reduced part a symmetric and complete fO_2 diffusion profile is observed (Figure 2d). fO_2 in oxidized part is lowered by 1.3 log units in general. SEM observation revealed that magnetite corona enclosing Pt alloys almost disappeared after diffusion annealing and the amount of small scattering magnetite particles in matrix reduced significantly (Supplementary Figure S7 in Supporting Information S1). The significantly shifted Matano interface (Figure 3d) could be caused by the fact that decomposition of magnetite is much faster than reduction of olivine, resulting in larger kinetic contrast compared with magnetite-free couple. The calculated diffusion coefficient lies on the fitting line of magnetite-free couples (Figure 5), which indicates the same redox mechanism with that in reduced part of magnetite-free one.

4. Discussion

4.1. Redox Mechanisms of Olivine Aggregates

Magnesium site in olivine is strongly incompatible to trivalent ions (e.g., Fe^{3+}) while more compatible to divalent ion with similar size of Mg^{2+} (e.g., Fe^{2+}). Thus, oxidized olivine with large amount of Fe^{3+} would be more sensitive to changing fO_2 due to its structural instability, which resulted in faster re-equilibrium during electrical conductivity and isothermal relaxation measurements (Ullrich & Becker, 2001; Wanamaker & Duba, 1993). A four-times faster reduction rate that corresponds to 0.6 log unit difference in diffusivity compared with oxidation rate is also demonstrated in our present study (Figure 4). Therefore, oxidation and reduction processes in olivine are probably governed by different mechanisms in magnetite-free couple.

In this study, diffusion coefficients obtained at 1,373–1,573 K during oxidation process in the reduced part below NNO buffer are in the range of $10^{-11.5}$ – $10^{-13.5}$ m^2/s with ΔH of 235 ± 56 kJ/mol (Figure 5). Oxygen lattice diffusion coefficient on the order of 10^{-18} to 10^{-20} m^2/s (Costa & Chakraborty, 2008; Dohmen et al., 2002; Fei, Wiedenbeck, et al., 2018) can be excluded due to its extremely slow diffusivity (Figure 6). Because of apparent involvement of Fe and Mg, Fe-Mg interdiffusion from previous studies are also plotted for comparison (Figure 6). ΔH averaged from geometric mean value of three axes ranges from 177 to 301 kJ/mol (Dohmen et al., 2007; Jurewicz & Watson, 1988; Nakamura & Schmalzried, 1984), which is similar to that obtained in this study. But their diffusivities are 2.5–6 orders of magnitude slower. H_2O in olivine was shown to increase Fe-Mg interdiffusivity by approximately 1.5 orders (Hier-Majumder et al., 2005). However, it is difficult to compensate for the large gap, given the extremely low H_2O in the present study (Figure S4 in Supporting Information S1). Besides, factor of fO_2 dependence which is between 1/4 and 1/6 for Fe-Mg interdiffusion (Dohmen et al., 2007) also contradicts with fO_2 -independent property here. Thus, Fe-Mg interdiffusion is unfavorable for oxidation process.

Diffusivity of Mg grain boundary diffusion (GBD) is comparable to oxidation rate (Figure 6). However, it had high ΔH (376 kJ/mol) when trace amount of hydrogen existed (Farver et al., 1994). In Arrhenius

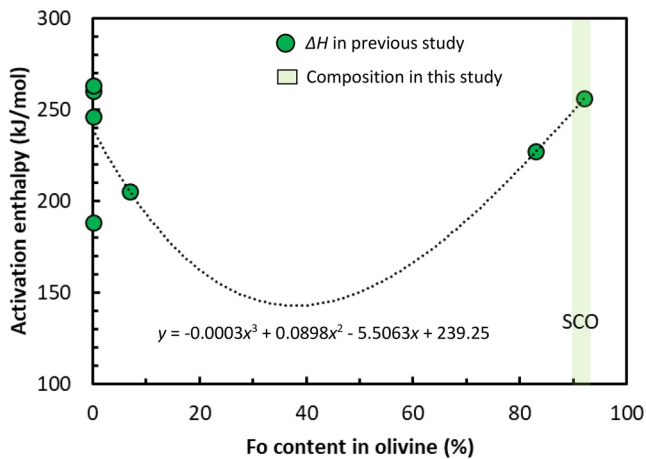


Figure 7. ΔH of reduction process in olivine versus forsterite component from previous studies. Dotted line is polynomial fitting of composition-dependent ΔH with fitting equation marked below it. Light green region indicates ΔH range of San Carlos olivine. For more detail, see in Supporting Information S1.

equation, similar pre-exponential factors relate to comparable atomic jump distance or frequency, while different activation enthalpies usually suggest different diffusion mechanisms. Thus Mg GBD can be ruled out as the dominant mechanism. For oxygen GBD in forsterite (Condit et al., 1985), when the effective grain boundary width in previous study is corrected to 1 nm (Dohmen & Milke, 2010), it is on the order of 10^{-12} m²/s, consistent with diffusivity in oxidation process in the present study. However, its ΔH was previously reported as 367 ± 314 kJ/mol with significant error (Condit et al., 1985). If two abnormally high diffusivities related to melt or penetration of oxygen along cracks were removed, the other two remaining points yield ΔH of 324 kJ/mol, which is only a little bit larger than that in oxidation process (235 ± 56 kJ/mol) in this study. This discrepancy might be due to their extremely rare data points or the absence of iron in their sample used for oxygen GBD (Condit et al., 1985). Diffusivity of the same order was also found for Fe loss from San Carlos olivine to metal capsule (Faul et al., 2017), which was also ascribed to oxygen GBD. The produced O₂ diffused into sample and resulted in similar fO_2 profile observed in this study (Figure 2). Therefore, we expect that oxidation process in reduced part of diffusion couple is driven by oxygen GBD, with O₂ source originating from the reduction of olivine in its counter oxidized part.

For reduction process above NNO buffer whose diffusivity is up to 0.6 log unit higher, its ΔH cannot be determined from the present study. In the absence of solid graphite, CO and H₂ gas, reduction process of San Carlos olivine could be controlled by diffusion in the bulk (Ullrich & Becker, 2001). When a same mechanism is assumed, ΔH for reduction process in previous studies exhibits a parabolic relationship with respect to forsterite content in olivine (Figure 7). It yields an estimated ΔH of ~ 250 kJ/mol for reduction of San Carlos olivine (Fo₉₂) used in this study. With elevated diffusivity compared with oxidation process, the possible dominating diffusing species in reduction process might be hydrogen related with Mg vacancy whose ΔH is about 274 kJ/mol (Padrón-Navarta et al., 2014). It was shown that even the water content was extremely small on Mg site (<10 wt. ppm), hydrous defects related to Mg vacancy could diffuse on the order of $10^{-11.7}$ at 1473 K. Reactions with the opposite direction below (Faul et al., 2017):



minimizes the concentration of metal vacancies, resulting in a slight shrink of crystal volume and thus visible grain boundaries (Figures 1c and 1d). Moisture trapped at the contact interface diffuses into olivine crystal through grain boundaries, which in turn facilitates redox process in the oxidized part, resulting in hydrogen diffusion-controlled redox mechanism. The strong fO_2 dependence here could attribute to different site occupancies for hydrogen diffusing species in order to meet charge neutrality conditions (Nishihara et al., 2008).

fO_2 -dependent oxidation is also observed above NNO buffer at 1473 K in magnetite-free couple, whose diffusion coefficient connects with that in reduction process smoothly (points marked 5 hr in Figure 4), implying a same mechanism with reduction process above NNO buffer, that is, hydrogen diffusion related with Mg site. Therefore, it seems that the real-time fO_2 during diffusion annealing plays the decisive role in determining redox mechanism, whose cut-off point is around NNO buffer (between $\Delta FMQ + 0.5$ and $+ 1$). However, in magnetite-bearing couple, oxygen GBD dominates across the whole fO_2 range investigated, regardless of real-time fO_2 . One possibility to explain this inconsistency is that O₂ produced by reduction of magnetite fills grain boundaries of olivine aggregate before hydrogen is supplied from the contact interface.

In summary, redox process in magnetite-free olivine aggregate is controlled by oxygen GBD below $\Delta FMQ + 1$ buffer, while it is rate-limited by faster diffusion species which might be hydrogen related Mg vacancy above $\Delta FMQ + 1$. For the magnetite-bearing couple, oxygen GBD dominates across all the investigated fO_2 range.

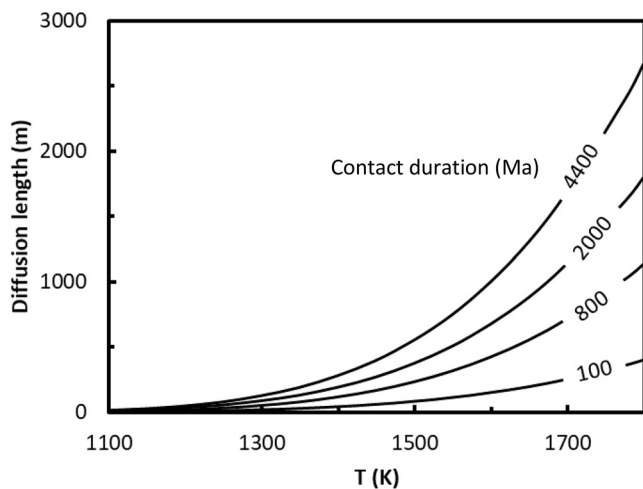


Figure 8. Oxidation length of the upper mantle as a function of temperature corresponding to geotherm at different depths. Numbers indicate the accumulative contact duration of slab with the surrounding upper mantle.

4.2. Implications for Oxidation Extent of the Upper Mantle by Slab and Possible Oxygen Budget in Deep Earth

Oxidized subducting slab has the ability to alter redox state of reducing mantle as an oxidant. However, its redox state as well as that of mantle wedge can be changed due to migration of fluids released by dehydration reactions within slab at the initial stage of subduction. One index to evaluate redox state of slab and mantle wedge is Fe valence state. Chen et al. (2019) suggested that significant amount of Fe^{3+} in the mantle wedge was reduced to Fe^{2+} by reducing fluid derived from dehydration of serpentinite. On the contrary, some studies showed that dehydration of serpentinite can release more oxidized fluids (Debret et al., 2015; Evans et al., 2017), which played an opposite role to oxidize Fe^{2+} . At this moment, it is difficult to evaluate how much these dehydration reaction processes vary redox budget of subducting slab. But even if we assume that the amount of Fe^{3+} reduced in slab outweighs that of Fe^{2+} oxidized, the extremely low solubility of Fe in NaCl solution (<0.01 M; Althaus & Johannes, 1969; Khodorevskaya & Aranovich, 2016; Wykes et al., 2008) makes the influence of such reactions on redox state of slabs negligible. Recent studies revealed that other multi-valence elements such as S and C are mostly retained within slab (Galvez et al., 2013; Piccoli et al., 2019), demonstrating little effect on the change of redox state of slab. Therefore, the subducted slab may maintain an oxidized state after the major dehydration process.

Spinel or garnet peridotite assemblages of xenoliths from subduction settings show $f\text{O}_2$ from $\Delta\text{FMQ} + 1.5$ to -1 (Frost & McCammon, 2008). $f\text{O}_2$ of surrounding upper mantle, which is mainly constituted by olivine and pyroxene, varies from FMQ equilibrium to $\Delta\text{IW}-1.5$ (Rohrbach & Schmidt, 2011). Thus, there will be redox process between the upper mantle and subducting slab and the former will be oxidized by the latter through oxygen GBD in olivine (see Discussion Section 4.1 for detail). Since slab continues subducting at a steady rate in the present Earth (Butterworth et al., 2014), it can be treated as an oxygen supplier with nearly constant $f\text{O}_2$ which can continuously oxidize the contacting surrounding mantle. Oxidation extent of the upper mantle at certain depth can thus be acquired by calculating diffusion length using the equation $L = 2\sqrt{Dt}$ where D is the diffusion coefficient and t is the contact duration between mantle and subducting slab, when temperature is known (Figure 8). The effect of pressure on redox kinetics was not considered. The oxygen GBD could have negative pressure dependence as well as other elements in olivine (Farver et al., 1994; Fei, Koizumi, et al., 2018). Thus, extrapolation of our data to high pressure would yield the upper limit of oxidation length in the upper mantle when temperature at the 410-seismic discontinuity was fixed at 1830 K for the normal mantle adiabat geotherm (Katsura et al., 2010). When slab passes through this depth for 100 Ma, only 462 m of the upper mantle can be oxidized. Even if slab starts subduction and passing through the upper mantle for 4.5 Gyrs, the maximum diffusion length is less than 4 km (Figure 8). As surface temperature of real slab is much lower than normal mantle geotherm used above, diffusion process will contribute even less to the oxidation extent of the upper mantle under water-undersaturated condition. This explains why $f\text{O}_2$ of the uppermost mantle is rarely changed over past 3.5 Gyrs (Canil, 2002; Li & Lee, 2004). That is, the unchanged $f\text{O}_2$ of the uppermost mantle in the past geological time is due to extremely sluggish redox process rather than the speculation that mantle serves as an infinite redox buffer.

Recent stratigraphic and geochemical studies suggested that some relicts of subducted material operated 4.4 or 3.8 Gyrs ago (Turner et al., 2014). Episodic subduction till 2.1 Gyrs (Liu et al., 2019) and extremely dynamic mantle convective flow prevents slab from reaching deep Earth and renders redox process between deep upper mantle and subducting slab insufficient, which further decreases the diffusion length and redox budget in slab consumed by the uppermost mantle. Therefore, redox budget could have been retained within ancient slab fragments which resulted in contrastingly different $f\text{O}_2$ signatures observed in mid-ocean ridge basalts (MORBs; Bryndzia et al., 1989; Cottrell & Kelley, 2011; Lee et al., 2005), coupled with other geochemical signatures such as Os, Sr, Pb, and Nd isotopes in mantle heterogeneities due to slow diffusion processes (Kogiso et al., 2004).

The slow redox process prevents subducting slab from being efficiently reduced, which suggests that it can transport oxidized components to the mantle transition zone or the lower mantle as an effective oxidant as indicated

by seismic tomography (Fukao & Obayashi, 2013). To calculate the total redox budget brought by Fe in slab, it is reasonable to define metallic phase as the reference since fO_2 in the deep upper mantle is below IW equilibrium from beyond 8 GPa (~240 km; Rohrbach & Schmidt, 2011). Assuming (a) total length of subduction zone is 44,450 km (Jarrard, 2003); (b) average subduction rate is 13 mm/y (Butterworth et al., 2014); (c) olivine is the main mineral in unserpentinised lithospheric mantle with Mg# equals to 90; (d) Fe^{3+} content in olivine is negligible, Fe^{2+} flux in 100 km-thick unserpentinised lithospheric mantle is calculated to be 156.4×10^{12} mol/y. Previous study showed that Fe^{3+} and Fe^{2+} fluxes from sediments, crust and serpentinized lithosphere were 15×10^{12} and 39.6×10^{12} mol/y respectively (Evans, 2012). Therefore, a total Fe^{2+} flux of 196×10^{12} mol/y and Fe^{3+} flux of 15×10^{12} mol/y are obtained. Since metallic phase is defined as the reference state, both Fe^{3+} and Fe^{2+} contribute to redox budget of Fe in slab. In the present study, it is the total amounts of electrons required to bring both Fe^{2+} and Fe^{3+} to metallic phase, where 2 mol of electrons are required for Fe^{2+} and 3 mol for Fe^{3+} , respectively. Therefore, total redox budget from Fe flux in slab is 437.1×10^{12} mol/y. It gives the maximum amount that slab can bring to deeper Earth, which is equivalent to 109.3×10^{12} mol/y oxygen gas (O_2). If magnetite which contributes most of Fe^{3+} decomposes at shallow depth before reduction process operates in olivine aggregate as indicated by magnetite-bearing couple (Figure 2d), the redox budget brought into deep Earth will decrease to 392×10^{12} mol/y, which is equivalent to 98×10^{12} mol/y O_2 . If minerals at the transition zone fails to absorb most of oxidized components in slab, a highly underestimated oxygen reservoir could be present in the lower mantle, as indicated by P-wave tomography that some slabs descend well into the deep lower mantle (Fukao and Obayashi., 2013). If oxidized components reach the core-mantle boundary, it may contribute to negative tungsten isotopes recorded by ocean island basalts (OIBs) such as Iceland and Hawaii (Mundl et al., 2017; Yoshino et al., 2020).

5. Conclusions

We investigated redox kinetics of olivine adopting diffusion couple method at 1 GPa and 1,373–1,573 K using a piston cylinder apparatus. It is found that redox process in olivine is diffusion-controlled, and diffusing on the order of 10^{-12} m²/s at 1,473 K. Oxidation process in the initially reduced olivine (IW buffered) is oxygen fugacity (fO_2)-independent with activation enthalpy of 235 ± 56 kJ/mol. Reduction process in the initially oxidized olivine (NNO buffered) is fO_2 -dependent with an fO_2 exponent of 2/5. Diffusion profile analysis reveals that below $\Delta FMQ + 1$, redox process in olivine is controlled by oxygen GBD, while above $\Delta FMQ + 1$, it is rate-limited by faster diffusion species which might be hydrogen related Mg vacancy. For magnetite-bearing couple whose diffusion profile only exists in the initially reduced part, oxygen GBD controls oxidation process over the whole fO_2 range investigated.

Oxidation extent of the upper mantle at certain depth can be acquired by calculating diffusion length resulted from redox kinetics of olivine. When slab passes through the lowermost upper mantle just at atop of the transition zone for 100 Ma, only 462 m of the surrounding mantle can be oxidized. Even if slab starts subduction and passing through the upper mantle for 4.5 Gyrs, the maximum diffusion length is less than 4 km. The extremely sluggish redox process explains why fO_2 of the uppermost mantle is rarely changed over past 3.5 Gyrs. Redox budget could have been retained within slab fragments which resulted in contrastingly different fO_2 signatures observed in mid-ocean ridge basalts (MORBs). When slab subducts into the lower mantle as indicated by P-wave tomography, a highly underestimated oxygen reservoir could have been formed if minerals at the mantle transition zone fails to absorb most of oxidized components brought by slab.

Data Availability Statement

The EPMA data set generated during the current study are available at DOI: <https://10.17605/OSF.IO/WMZKB>.

References

- Althaus, E., & Johannes, W. (1969). Experimental metamorphism of NaCl-bearing aqueous solutions by reactions with silicates. *American Journal of Science*, 267, 87–98. <https://doi.org/10.2475/ajs.267.1.87>
- Brounce, M., Cottrell, E., & Kelley, K. A. (2019). The redox budget of the Mariana subduction zone. *Earth and Planetary Science Letters*, 528, 115859. <https://doi.org/10.1016/j.epsl.2019.115859>
- Brounce, M., Kelley, K. A., Cottrell, E., & Reagan, M. K. (2015). Temporal evolution of mantle wedge oxygen fugacity during subduction initiation. *Geology*, 43, 775–778. <https://doi.org/10.1130/g36742.1>

Acknowledgments

The authors thank Koga Kenneth, D. Yamazaki and N. Tsujino for their discussion, and N. Tsujino for help of IR measurement. This work was supported by the Ministry of Education, Culture, Sports, Science, and Technology of the Japanese Government, Grant Numbers, 17H01155 to T. Yoshino, and partially supported by NSFC (41973056) and CPSF (2021M702790).

- Brounce, M. N., Kelley, K. A., & Cottrell, E. (2014). Variations in $\text{Fe}^{3+}/\Sigma\text{Fe}$ of Mariana arc basalts and mantle wedge f_{O_2} . *Journal of Petrology*, 55, 2513–2536. <https://doi.org/10.1093/ptrology/egu065>
- Bryndzia, L. T., Wood, B. J., & Dick, H. J. B. (1989). The oxidation state of the Earth's sub-oceanic mantle from oxygen thermobarometry of abyssal spinel peridotites. *Nature*, 341, 526–527. <https://doi.org/10.1038/341526a0>
- Butterworth, N. P., Talsma, A. S., Müller, R. D., Seton, M., Bunge, H. P., Schuberth, B. S. A., et al. (2014). Geological, tomographic, kinematic and geodynamic constraints on the dynamics of sinking slabs. *Journal of Geodynamics*, 73, 1–13. <https://doi.org/10.1016/j.jog.2013.10.006>
- Canil, D. (2002). Vanadium in peridotites, mantle redox and tectonic environments: Archean to present. *Earth and Planetary Science Letters*, 195, 75–90. [https://doi.org/10.1016/S0012-821X\(01\)00582-9](https://doi.org/10.1016/S0012-821X(01)00582-9)
- Chakraborty, S., Farver, J. R., Yund, R. A., & Rubie, D. C. (1994). Mg tracer diffusion in synthetic forsterite and as a function of P, T and f_{O_2} . *Physics and Chemistry of Minerals*, 21, 489–500. <https://doi.org/10.1007/bf00203923>
- Chen, Y.-X., Lu, W., He, Y., Schertl, H.-P., Zheng, Y.-F., Xiong, J.-W., & Zhou, K. (2019). Tracking Fe mobility and Fe speciation in subduction zone fluids at the slab-mantle interface in a subduction channel: A tale of whiteschist from the western Alps. *Geochimica et Cosmochimica Acta*, 267, 1–16. <https://doi.org/10.1016/j.gca.2019.09.020>
- Condit, R. H., Weed, H. C., & Piwinski, A. J. (1985). A technique for observing oxygen diffusion along grain boundary regions in synthetic forsterite. In R. N. Schock (Ed.), *Point defects in minerals, Geophysical Monograph series* (Vol. 31, pp. 97–105). American Geophysical Union.
- Costa, F., & Chakraborty, S. (2008). The effect of water on Si and O diffusion rates in olivine and implications for transport properties and processes in the upper mantle. *Physics of the Earth and Planetary Interiors*, 166, 11–29. <https://doi.org/10.1016/j.pepi.2007.10.006>
- Cottrell, E., & Kelley, K. A. (2011). The oxidation state of Fe in MORB glasses and the oxygen fugacity of the upper mantle. *Earth and Planetary Science Letters*, 305, 270–282. <https://doi.org/10.1016/j.epsl.2011.03.014>
- Debret, B., Bolfan-Casanova, N., Padrón-Navarta, J. A., Martín-Hernández, F., Andreani, M., Garrido, C. J., et al. (2015). Redox state of iron during high-pressure serpentinite dehydration. *Contributions to Mineralogy and Petrology*, 169, 36. <https://doi.org/10.1007/s00410-015-1130-y>
- Dohmen, R., Becker, H.-W., & Chakraborty, S. (2007). Fe-Mg diffusion in olivine I: Experimental determination between 700 and 1,200°C as a function of composition, crystal orientation and oxygen fugacity. *Physics and Chemistry of Minerals*, 34, 389–407. <https://doi.org/10.1007/s00269-007-0157-7>
- Dohmen, R., Chakraborty, S., & Becker, H.-W. (2002). Si and O diffusion in olivine and implications for characterizing plastic flow in the mantle. *Geophysical Research Letters*, 29(21), 2030. <https://doi.org/10.1029/2002GL015480>
- Dohmen, R., & Milke, R. (2010). Diffusion in polycrystalline materials: Grain boundaries, mathematical models, and experimental data. *Reviews in Mineralogy and Geochemistry*, 72, 921–970. <https://doi.org/10.2138/rmg.2010.72.21>
- Evans, K. A. (2006). Redox decoupling and redox budgets: Conceptual tools for the study of earth systems. *Geology*, 34, 489–492. <https://doi.org/10.1130/g22390.1>
- Evans, K. A. (2012). The redox budget of subduction zones. *Earth-Science Reviews*, 113, 11–32. <https://doi.org/10.1016/j.earscirev.2012.03.003>
- Evans, K. A., & Powell, R. (2015). The effect of subduction on the sulphur, carbon and redox budget of lithospheric mantle. *Journal of Metamorphic Geology*, 33, 649–670. <https://doi.org/10.1111/jmg.12140>
- Evans, K. A., Reddy, S. M., Tomkins, A. G., Crossley, R. J., & Frost, B. R. (2017). Effects of geodynamic setting on the redox state of fluids released by subducted mantle lithosphere. *Lithos*, 278–281, 26–42. <https://doi.org/10.1016/j.lithos.2016.12.023>
- Evans, K. A., & Tomkins, A. G. (2011). The relationship between subduction zone redox budget and arc magma fertility. *Earth and Planetary Science Letters*, 308, 401–409. <https://doi.org/10.1016/j.epsl.2011.06.009>
- Farver, J. R., & Yund, R. A. (2000). Silicon diffusion in forsterite aggregates: Implications for diffusion accommodated creep. *Geophysical Research Letters*, 27(15), 2337–2340. <https://doi.org/10.1029/2000gl008492>
- Farver, J. R., Yund, R. A., & Rubie, D. C. (1994). Magnesium grain boundary diffusion in forsterite aggregates at 1000°–1300°C and 0.1 MPa to 10 GPa. *Journal of Geophysical Research*, 99(B10), 19809–19819. <https://doi.org/10.1029/94jb01250>
- Faul, U. H., Cline, C. J., Berry, A., Jackson, I., & Garapić, G. (2017). Constraints on oxygen fugacity within metal capsules. *Physics and Chemistry of Minerals*, 45, 497–509. <https://doi.org/10.1007/s00269-017-0937-7>
- Fei, H., Koizumi, S., Sakamoto, N., Hashiguchi, M., Yurimoto, H., Marquardt, K., et al. (2016). New constraints on upper mantle creep mechanism inferred from silicon grain-boundary diffusion rates. *Earth and Planetary Science Letters*, 433, 350–359. <https://doi.org/10.1016/j.epsl.2015.11.014>
- Fei, H., Koizumi, S., Sakamoto, N., Hashiguchi, M., Yurimoto, H., Marquardt, K., et al. (2018). Pressure, temperature, water content, and oxygen fugacity dependence of the Mg grain-boundary diffusion coefficient in forsterite. *American Mineralogist*, 103, 1354–1361. <https://doi.org/10.2138/am-2018-6480>
- Fei, H., Wiedenbeck, M., Sakamoto, N., Yurimoto, H., Yoshino, T., Yamazaki, D., & Katsura, T. (2018). Negative activation volume of oxygen self-diffusion in forsterite. *Physics of the Earth and Planetary Interiors*, 275, 1–8. <https://doi.org/10.1016/j.pepi.2017.12.005>
- Frost, D. J., & McCammon, C. A. (2008). The redox state of Earth's mantle. *Annual Review of Earth and Planetary Sciences*, 36, 389–420. <https://doi.org/10.1146/annurev.earth.36.031207.124322>
- Fukao, Y., & Obayashi, M. (2013). Subducted slabs stagnant above, penetrating through, and trapped below the 660 km discontinuity. *Journal of Geophysical Research*, 118, 5920–5938. <https://doi.org/10.1002/2013jb010466>
- Galvez, M. E., Beyssac, O., Martinez, I., Benzerara, K., Chaduteau, C., Malvoisin, B., & Malavieille, J. (2013). Graphite formation by carbonate reduction during subduction. *Nature Geoscience*, 6, 473–477. <https://doi.org/10.1038/ngeo1827>
- Gorman, P. J., Kerrick, D. M., & Connolly, J. A. D. (2006). Modeling open system metamorphic decarbonation of subducting slabs. *Geochemistry, Geophysics, Geosystems*, 7(4), Q04007. <https://doi.org/10.1029/2005GC001125>
- Hier-Majumder, S., Anderson, I. M., & Kohlstedt, D. L. (2005). Influence of protons on Fe-Mg interdiffusion in olivine. *Journal of Geophysical Research*, 110, B02202. <https://doi.org/10.1029/2004JB003292>
- Jarrard, R. D. (2003). Subduction fluxes of water, carbon dioxide, chlorine, and potassium. *Geochemistry, Geophysics, Geosystems*, 4(5), 8905. <https://doi.org/10.1029/2002GC000392>
- Jurewicz, A. J. G., & Watson, E. B. (1988). Cations in olivine, Part 2: Diffusion in olivine xenocrysts, with applications to petrology and mineral physics. *Contributions to Mineralogy and Petrology*, 99, 186–201. <https://doi.org/10.1007/bf00371460>
- Kadik, A. (1997). Evolution of Earth's redox state during upwelling of carbon-bearing mantle. *Physics of the Earth and Planetary Interiors*, 100, 157–166. [https://doi.org/10.1016/S0031-9201\(96\)03237-2](https://doi.org/10.1016/S0031-9201(96)03237-2)
- Kasting, J. F., Egger, D. H., & Raeburn, S. P. (1993). Mantle redox evolution and the oxidation state of the Archean atmosphere. *The Journal of Geology*, 101(2), 245–257. <https://doi.org/10.1086/648219>
- Katsura, T., Yoneda, A., Yamazaki, D., Yoshino, T., & Ito, E. (2010). Adiabatic temperature profile in the mantle. *Physics of the Earth and Planetary Interiors*, 183, 212–218. <https://doi.org/10.1016/j.pepi.2010.07.001>

- Kelley, K. A., & Cottrell, E. (2009). Water and the oxidation state of subduction zone magmas. *Science*, 325, 605–607. <https://doi.org/10.1126/science.1174156>
- Kerrick, D. M., & Connolly, J. A. D. (2001). Metamorphic devolatilization of subducted marine sediments and the transport of volatiles into the Earth's mantle. *Nature*, 411, 293–296. <https://doi.org/10.1038/35077056>
- Khodorevskaya, L. I., & Aranovich, L. Y. (2016). Experimental study of amphibole interaction with H₂O-NaCl Fluid at 900°C, 500 MPa: Toward granulite facies melting and mass transfer. *Petrology*, 24(3), 235–254. <https://doi.org/10.1134/s0869591116030036>
- Kogiso, T., Hirschmann, M. M., & Reiners, P. W. (2004). Length scales of mantle heterogeneities and their relationship to ocean island basalt geochemistry. *Geochimica et Cosmochimica Acta*, 68(2), 345–360. [https://doi.org/10.1016/s0016-7037\(03\)00419-8](https://doi.org/10.1016/s0016-7037(03)00419-8)
- Lécuyer, C., & Ricard, Y. (1999). Long-term fluxes and budget of ferric iron: Implication for the redox states of the Earth's mantle and atmosphere. *Earth and Planetary Science Letters*, 165, 197–211. [https://doi.org/10.1016/s0012-821x\(98\)00267-2](https://doi.org/10.1016/s0012-821x(98)00267-2)
- Lee, C.-T. A., Leeman, W. P., Canil, D., & Li, Z.-X. A. (2005). Similar V/Sc systematics in MORB and arc basalts: Implications for the oxygen fugacities of their mantle source regions. *Journal of Petrology*, 46(11), 2313–2336. <https://doi.org/10.1093/ptrology/egi056>
- Lee, C.-T. A., Luffi, P., Le Roux, V., Dasgupta, R., Albarede, F., & Leeman, W. P. (2010). The redox state of arc mantle using Zn/Fe systematics. *Nature*, 468, 681–685. <https://doi.org/10.1038/nature09617>
- Li, Z.-X. A., & Lee, C.-T. A. (2004). The constancy of upper mantle f_{O2} through time inferred from V/Sc ratios in basalts. *Earth and Planetary Science Letters*, 228, 483–493. <https://doi.org/10.1016/j.epsl.2004.10.006>
- Liu, H., Sun, W. D., Zartman, R., & Tang, M. (2019). Continuous plate subduction marked by the rise of alkali magmatism 2.1 billion years ago. *Nature Communications*, 10, 3408. <https://doi.org/10.1038/s41467-019-11329-z>
- Matano, C. (1933). On the relation between the diffusion coefficients and concentrations of solid metals (the nickel-copper system). *Japanese Journal of Physics*, 8, 109–113.
- Mendelson, M. I. (1969). Average grain size in polycrystalline ceramics. *Journal of the American Ceramic Society*, 52(8), 443–446. <https://doi.org/10.1111/j.1151-2916.1969.tb11975.x>
- Mundl, A., Touboul, M., Jackson, M. G., Day, J. M. D., Kurz, M. D., Lekic, V., et al. (2017). Tungsten-182 heterogeneity in modern ocean island basalts. *Science*, 356, 66–69. <https://doi.org/10.1126/science.aal4179>
- Nakamura, A., & Schmalzried, H. (1984). On the Fe²⁺-Mg²⁺-interdiffusion in olivine (II). *Berichte der Bunsen-Gesellschaft für Physikalische Chemie*, 88, 140–145. <https://doi.org/10.1002/bbpc.19840880212>
- Nishihara, Y., Shinmei, T., & Karato, S.-I. (2008). Effect of chemical environment on the hydrogen-related defect chemistry in wadsleyite. *American Mineralogist*, 93, 831–843. <https://doi.org/10.2138/am.2008.2653>
- Padrón-Navarta, J. A., Hermann, J., & O'Neill, H. S. C. (2014). Site-specific hydrogen diffusion rates in forsterite. *Earth and Planetary Science Letters*, 392, 100–112. <https://doi.org/10.1016/j.epsl.2014.01.055>
- Parkinson, I. J., & Arculus, R. J. (1999). The redox state of subduction zones: Insights from arc-peridotites. *Chemical Geology*, 160, 409–423. [https://doi.org/10.1016/s0009-2541\(99\)00110-2](https://doi.org/10.1016/s0009-2541(99)00110-2)
- Paterson, M. S. (1982). The determination of hydroxyl by infrared absorption in quartz, silicate glasses and similar materials. *Bulletin de Mineralogie*, 105, 20–29. <https://doi.org/10.3406/bulmi.1982.7582>
- Piccoli, F., Hermann, J., Pettke, T., Connolly, J. A. D., Kempf, E. D., & Duarte, J. F. V. (2019). Subducting serpentinites release reduced, not oxidized, aqueous fluids. *Scientific Reports*, 9. <https://doi.org/10.1038/s41598-019-55944-8>
- Rohrbach, A., & Schmidt, M. W. (2011). Redox freezing and melting in the Earth's deep mantle resulting from carbon-iron redox coupling. *Nature*, 472, 209–212. <https://doi.org/10.1038/nature09899>
- Rupke, L. H., Morgan, J. P., Hort, M., & Connolly, J. A. D. (2004). Serpentine and the subduction zone water cycle. *Earth and Planetary Science Letters*, 223, 17–34. <https://doi.org/10.1016/j.epsl.2004.04.018>
- Schwarzenbach, E. M., Caddick, M. J., Petroff, M., Gill, B. C., Cooperdock, E. H. G., & Barnes, J. D. (2018). Sulphur and carbon cycling in the subduction zone melange. *Scientific Reports*, 8, 15517. <https://doi.org/10.1038/s41598-018-33610-9>
- Sverjensky, D. A., Stagno, V., & Huang, F. (2014). Important role for organic carbon in subduction-zone fluids in the deep carbon cycle. *Nature Geoscience*, 7, 909–913. <https://doi.org/10.1038/NGEO2291>
- Turner, S., Rushmer, T., Reagan, M., & Moya, J. F. (2014). Heading down early on? Start of subduction on earth. *Geology*, 42, 139–142. <https://doi.org/10.1130/G34886.1>
- Ullrich, K., & Becker, K. D. (2001). Kinetics and diffusion of defects in fayalite. Fe₂SiO₄. *Solid State Ionics*, 141–142, 307–312. [https://doi.org/10.1016/s0167-2738\(01\)00796-2](https://doi.org/10.1016/s0167-2738(01)00796-2)
- Wanamaker, B. J., & Duba, A. G. (1993). Electrical conductivity of San Carlos Olivine along [100] under oxygen- and pyroxene-buffered conditions and implications for defect equilibria. *Journal of Geophysical Research*, 98(B1), 489–500. <https://doi.org/10.1029/92jb01584>
- Wykes, J. L., Newton, R. C., & Manning, C. E. (2008). Solubility of andradite, Ca₃Fe₂Si₃O₁₂, in a 10 mol% NaCl solution at 800°C and 10kbar: Implications for the metasomatic origin of grandite garnet in calc-silicate granulites. *American Mineralogist*, 93, 886–892.
- Yoshino, T., Makino, Y., Suzuki, T., & Hirata, T. (2020). Grain boundary diffusion of W in lower mantle phase with implications for isotopic heterogeneity in oceanic island basalts by core-mantle interactions. *Earth and Planetary Science Letters*, 530, 115887. <https://doi.org/10.1016/j.epsl.2019.115887>

References From the Supporting Information

- Gaballah, I., Jeannot, F., Gleitzer, C., & Dufour, L. C. (1975). Cinétique de réduction de l'orthosilicate de fer Fe₂SiO₄ (fayalite) par H₂, CO et les mélanges CO+H₂. *Mém. Sci. Rev. Métallurg.*
- Khisina, N. R., Khramov, D. A., Kleschev, A. A., & Langer, K. (1998). Laihunitization as a mechanism of olivine oxidation. *European Journal of Mineralogy*, 10, 229–238. <https://doi.org/10.1127/ejm/10/2/0229>
- Khisina, N. R., Khramov, D. A., Kolosov, M. V., Kleschev, A. A., & Taylor, L. A. (1995). Formation of ferriolivine and magnesioferrite from Mg-Fe olivine reactions and kinetics of oxidation. *Physics and Chemistry of Minerals*, 22, 241–250. <https://doi.org/10.1007/bf00202257>
- Mackwell, S. J. (1992). Oxidation kinetics of fayalite (Fe₂SiO₄). *Physics and Chemistry of Minerals*, 19, 220–228. <https://doi.org/10.1007/bf00202311>
- Massieon, C., Cutler, A., & Shadman, F. (1992). *Reduction of iron-bearing lunar minerals for the production of oxygen* (p. 106). Univrsity of Arizona (M.S thesis).
- Massieon, C., Cutler, A., & Shadman, F. (1993). Hydrogen reduction of iron-bearing silicates. *Industrial & Engineering Chemistry Research*, 32, 1239–1244. <https://doi.org/10.1021/ie00018a033>

- Minowa, S., Yamada, M., & Torii, Y. (1968). A study on the formation and reduction of fayalite (Fe_2SiO_4). *Tetsu to Hagane*, *54*, 1203–1216. https://doi.org/10.2355/tetsutohagane1955.54.12_1203
- Nagahara, H. (1986). Reduction kinetics of olivine and oxygen fugacity environment during chondrule formation. *Lunar and Planetary Science*, *17*, 595–596.
- Warczak, A., & Utigard, T. A. (1998). Fayalite slag reduction by solid graphite. *Canadian Metallurgical Quarterly*, *37*, 27–39. <https://doi.org/10.1179/cmq.1998.37.1.27>
- Woodland, A. B., & O'Neill, H. S. C. (1997). Thermodynamic data for Fe-bearing phases obtained using noble metal alloys as redox sensors. *Geochimica et Cosmochimica Acta*, *61*(20), 4359–4366. [https://doi.org/10.1016/s0016-7037\(97\)00247-0](https://doi.org/10.1016/s0016-7037(97)00247-0)
- Wu, T., & Kohlstedt, D. L. (1988). Rutherford backscattering spectroscopy study of the kinetics of oxidation of $(\text{Mg}, \text{Fe})_2\text{SiO}_4$. *Journal of the American Ceramic Society*, *71*, 540–545. <https://doi.org/10.1111/j.1151-2916.1988.tb05917.x>